small
NANO MICRO

Incremental Growth of Short SWNT Arrays by Pulsed Chemical Vapor Deposition

Alexander A. Puretzky, David B. Geohegan, Jeremy J. Jackson, Sreekanth Pannala, Gyula Eres, Christopher M. Rouleau, Karren L. More, Norbert Thonnard, and Jason D. Readle*

***V**ery short arrays of continuous single-wall carbon nanotubes (SWNTs) are grown incrementally in steps as small as 25 nm using pulsed chemical vapor deposition (CVD). In-situ optical extinction measurements indicate that over 98% of the nanotubes reinitiate growth on successive gas pulses, and high-resolution transmission electron microscopy (HR-TEM) images show that the SWNTs do not exhibit segments, caps, or noticeable sidewall defects resulting from repeatedly stopping and restarting growth. Time-resolved laser reflectivity (3-ms temporal resolution) is used to record the nucleation and growth kinetics for each fast (0.2 s) gas pulse and to measure the height increase of the array in situ, providing a method to incrementally grow short nanotube arrays to precise heights. Derivatives of the optical reflectivity signal reveal distinct temporal signatures for both nucleation and growth kinetics, with their amplitude ratio on the first gas pulse serving as a good predictor for the evolution of the growth of the nanotube ensemble into a coordinated array. Incremental growth by pulsed CVD is interpreted in the context of autocatalytic kinetic models as a special processing window in which a sufficiently high flux of feedstock gas drives the nucleation and rapid growth phases of a catalyst nanoparticle ensemble to occur within the temporal period of the gas pulse, but without inducing growth termination.*

1. Introduction

The unique morphology and anisotropic thermal and electrical conductivities of carbon nanotube arrays are enabling their application as thermal interfaces,[1–4] supercapacitors,[5,6] interconnects,[7] flexible electronics,[8,9] gas sensors,[10] optical absorbers,[11,12] adhesives,[13–15] foams,[16] and precursors for spun fibers and transparent conductive sheets.[17,18] While much effort has been devoted to prolonging the growth process of nanotube arrays by chemical vapor deposition (CVD) to produce array lengths of millimeters for bulk applications,[19–25] far less work has been devoted to the uniform growth of sub-micrometer arrays with precise lengths that could enable applications in sensors, microelectronics, organic electronics, and biology. It has been demonstrated that nanotubes can stop and restart growth when slow, continuous feedstock gas introduction is used in conventional CVD,[26–29] and very short (200–300 nm) single-wall carbon nanotube (SWNT) arrays have been grown using this approach.[26,30] However, this slow gas introduction is likely responsible for the lack of control over the nucleation and termination processes, resulting in a relatively high density of nanotubes that extend well above the nominal array length.[26,30]

Clearly, several processing requirements must be satisfied to enable the precise growth of short nanotube arrays by

Dr. A. A. Puretzky
Oak Ridge National Laboratory
Oak Ridge, TN 37831-6488, USA
E-mail: puretzkya@ornl.gov
Dr. D. B. Geohegan, Dr. J. J. Jackson, Dr. S. Pannala, Dr. G. Eres, Dr. C. M. Rouleau, Dr. K. L. More, Dr. N. Thonnard, Dr. J. D. Readle
Oak Ridge National Laboratory
Oak Ridge, TN 37831, USA

DOI: 10.1002/smll.201102173

CVD. First, a high nucleation efficiency should be achieved in order to produce the coordinated growth of a freestanding nanotube array. Since the growth of nanotube arrays by CVD is based on the cooperative response of a large number of catalyst nanoparticles typically having different diameters and catalytic activities, this requirement demands rapid activation of a relatively large subset of catalyst nanoparticles to provide enough nanotube areal density for the support of a coordinated nanotube array by "crowding". Second, the nucleation time for all nanotubes should be reduced to a minimum in order to induce rapid entanglement, crowding, and coordinated array growth, thereby minimizing the region of low-density, randomly oriented nanotubes at the top of the nanotube array. Third, a means to terminate the growth of all nanotubes simultaneously should be provided in order to minimize the number of nanotubes that extend above the desired thickness. Finally, a means of measuring array height accurately in real-time must be provided with sufficient temporal resolution to control the growth process.

Recently, we developed a pulsed CVD method that combines fast-flowing, subsecond pulses of acetylene with in-situ time-resolved reflectivity (TRR) to understand the rapid growth of nanotube arrays induced by high-partial-pressure pulses of feedstock gas.[31,32] While considerable progress has been achieved using environmental high-resolution transmission electron microscopy (HR-TEM)[33–42] to understand the nanoscale processes inherent in nanotube growth at low pressures, including the shape and composition of individual nanoparticles,[40,42] in-situ diagnostics of the coordinated growth of nanotubes in arrays within typical CVD reactors are mainly based on optical techniques such as TRR,[26,43,44] absorbance,[30,45,46] Raman scattering,[47–50] and direct video imaging.[19,51,52] Of these techniques, only TRR has the temporal and spatial precision required to investigate pulsed CVD within subsecond gas pulses. TRR can measure interferometrically the height of the array as it grows while simultaneously measuring changes in the effective optical extinction coefficient, thereby revealing changes in the density of the array as it grows from catalyst particles on the substrate.[31,44]

Using pulsed CVD with in-situ TRR we discovered that several aspects of nanotube array growth are highly flux dependent. First, the induction time for nucleation and growth was found to decline with increasing acetylene flux over three orders of magnitude, enabling rapid growth of approximately micrometer-tall arrays in single 0.5-s pulses.[31,32] Second, the density of the arrays was also very sensitive to the feedstock flux, permitting the synthesis of banded, variable-density arrays.[31] Third, the diameters of the SWNTs in the arrays were highly dependent on the flux, with the small <2.5 nm-diameter SWNTs extinguished at high acetylene fluxes due to carbon overcoating of their corresponding, highly active catalyst nanoparticles.[32]

Here we explore pulsed CVD and in-situ TRR in an attempt to meet the aforementioned criteria for the incremental growth of short nanotube arrays with precise lengths. Exploration of this growth regime requires an understanding of nucleation and growth kinetics on fast, subsecond time scales, which to-date have not been measured, so real-time TRR is employed both as a highly sensitive measure of array height and fast kinetics. Much lower acetylene partial pressures are used than in previous studies[31,32] in order to generate growth increments 10–100 times smaller while in-situ TRR is employed to assess the nucleation efficiency and measure induction times for nucleation and growth.

We find that very short, coordinated arrays of continuous single-wall carbon nanotubes can be grown incrementally in steps as small as 25 nm using pulsed CVD. Over 98% of the nanotubes reinitiate growth on successive gas pulses, and the SWNTs do not exhibit segments, caps, or noticeable sidewall defects resulting from repeatedly stopping and restarting growth. The kinetics data reveals distinct temporal signatures for both nanotube nucleation and growth, with their amplitude ratio on the first gas pulse serving as a good predictor for the evolution of the growth of the nanotube ensemble into a coordinated array. Incremental growth by pulsed CVD is interpreted in the context of autocatalytic kinetic models[53,54] as a special processing window in which sufficiently high fluxes of feedstock gas drive the nucleation and rapid growth phases of a catalyst nanoparticle ensemble to occur within the temporal period of the gas pulse, without inducing growth termination.

2. Results and Discussion

To investigate fast growth kinetics during carbon nanotube array synthesis, we used pulsed feedstock gas introduction. In this approach, millisecond gas pulses of acetylene were injected every 10 s into a low-pressure, high-velocity flow of Ar/H_2, which broaden to yield ~0.2 s pulses of acetylene with variable peak partial pressures arriving to a vertically standing substrate within a typical tube furnace. The growth of nanotube arrays was monitored using TRR, which can exhibit Fabry–Perot oscillations depending on the growth mode.[26,44] The appearance of oscillations in TRR requires a top array surface with a roughness $<\lambda/4$, where λ is the wavelength of the reflected light at normal incidence, plus motion of this surface away from the substrate (due to increasing height because of coordinated growth). This coordinated growth mode occurs only at some critical density of nanotubes and typically results in a crowded assembly of nanotubes evolving perpendicular to the substrate with a uniform velocity. In this case the overall reflected intensity typically drops exponentially, in some cases by orders of magnitude depending on the terminal height of an array (see for example reference [44]). This coordinated growth mode is quite different from uncoordinated growth, where the density of nanotubes is so low that a tightly knit top surface does not develop, resulting in unaligned nanotubes of various heights and growth directions. In this case, the reflected laser signal does not show any oscillations, and saturates fairly quickly after relatively small drops in intensity.

Figure 1a shows in-situ TRR signals obtained during pulsed growth of nanotube arrays at different partial pressures of C_2H_2. All curves show clear Fabry–Perot oscillations punctuated by discrete steps. The oscillations result from interference between laser beams reflected from the top of the nanotube array and from the Si substrate, and are characteristic of coordinated array growth.[26,44] The

small 2012,
DOI: 10.1002/smll.201102173

small NANO MICRO

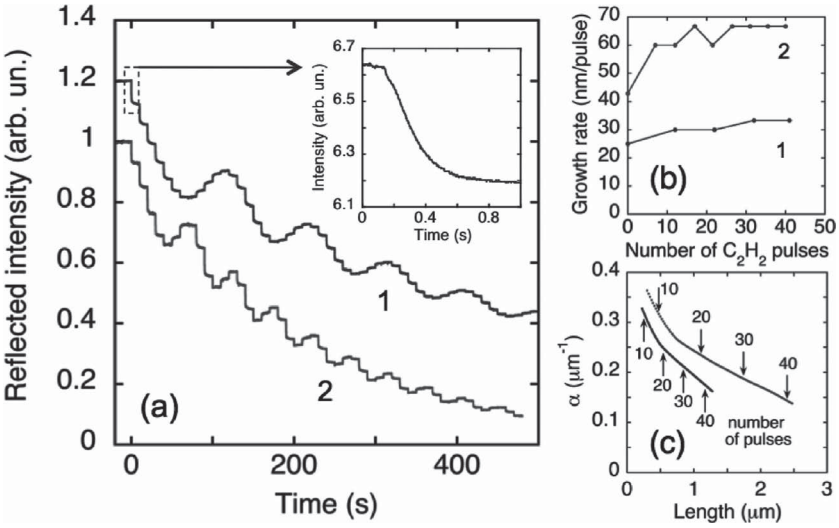

Figure 1. a) TRR signals corresponding to the incremental growth of 2 nanotube arrays grown at 720 °C with different peak partial pressures of C_2H_2, 0.16 Torr (curve 1) and 0.32 Torr (curve 2) (the backing C_2H_2 pressures were 20 and 40 psi, respectively). Curve 1 is offset by 0.2 from its maximum value of 1.0 for clarity. The inset shows the magnified view of the first pulse for curve 1. b) Growth rates of arrays versus the number of C_2H_2 pulses and c) extinction coefficients versus arrays length derived from curves 1 (lower traces) and 2 (upper traces). In both cases the growth is coordinated as indicated by the interference fringes.

steps correspond to subsecond increments in the height of the array (see inset), during which growth restarts and terminates, followed by ~9 s flushes of Ar/H_2 gas through the CVD reactor. The number of steps per oscillation gives a rapid estimate of the incremental growth per pulse. For example, at the smallest C_2H_2 partial pressure of 0.16 Torr (curve 1 in Figure 1a) it takes 12 C_2H_2 gas pulses to reach the first interference maximum (which corresponds to an array length of about 300 nm), yielding ~25 nm/pulse. The growth rates versus number of C_2H_2 pulses, and the absorption coefficients versus array length derived from these curves are shown in Figure 1b and c, respectively, and are described in references [31,44]. In the first case the growth rate is very low, ~25 nm/pulse, and increases only slightly to ~30 nm/pulse at the end. Increasing the partial pressure of C_2H_2 by a factor of 2 results in an increase of the corresponding growth rate to ~65 nm/pulse (Figure 1b). Interestingly, in both cases the extinction coefficients, which are directly related to the density of carbon within a nanotube array (see reference [31] for details), drop rapidly when the number of C_2H_2 pulses increases (Figure 1c). Since the growth rate per pulse is not decreasing, this decline in carbon density is most likely caused by a drop-off in the number of active catalyst nanoparticles that successfully reinitiate nanotube growth following each growth stoppage. Both curves in Figure 1c indicate that the nanotube array density drops a factor of 2 over 33 pulses, permitting an estimate for the fraction of nanotubes that regrow per pulse of ~0.98.

Figure 2a–c shows TEM and cross-sectional scanning electron microscopy (SEM) images of the array for which growth was monitored in Figure 1a (curve 1) at 720 °C with a peak C_2H_2 partial pressures of 0.16 Torr. According to the TEM images, this array contains mainly SWNTs with very small numbers of double-wall nanotubes (<1%). Analysis of high-resolution TEM images of carbon nanotubes from this array did not show any kinks, segments, or sidewall defects resulting from incremental growth of 25 nm per step. The lack of segments and caps is consistent with other observations during interrupted growth of SWNT arrays, wherein new caps were observed only on reheating, but not on the interruption of the feedstock gas.[27] The diameters of SWNTs estimated from TEM images range from 0.8 to 5 nm (Figure 2d). The corresponding Raman spectra for these nanotubes measured from the top of the array are shown in Figure 2e,f. These spectra confirm the presence of SWNTs with diameters from 0.8 to 2.5 nm in the array. Note that Raman spectra of the array from the top only show a subset of the actual nanotube distribution in the array.

The fast growth kinetics measured during our pulsed CVD approach revealed interesting new features in nanotube array nucleation and growth that are best understood in the context of **Figure 3**. Specifically, Figure 3a shows the TRR signal measured during pulsed growth of a ~300 nm-tall SWNT array using 5 C_2H_2 gas pulses. This curve exhibits pronounced steps corresponding to each gas pulse. The growth rate in this case is ~60 nm/pulse and the corresponding SEM image (Figure 3c) confirms the array height estimated from the reflectivity curve. To understand how the growth rate changes during the gas pulses, the first derivatives of the reflectivity curves, *dI*/*dt*, were analyzed and plotted in Figure 3b.

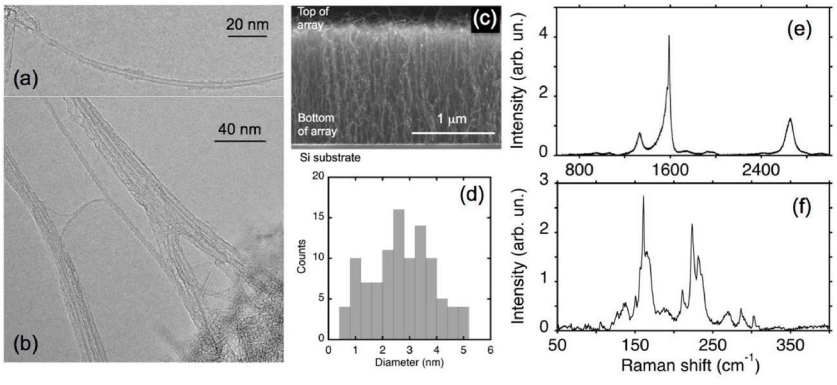

Figure 2. a,b) High-resolution TEM and c) cross-sectional SEM images of continuous single-wall carbon nanotubes grown incrementally using 55 pulses of C_2H_2 at 720 °C (corresponding reflectivity data - curve 1 Figure 1a). d) SWNT diameter distribution obtained from TEM. e,f) Raman spectra of the nanotube array measured at 532 nm excitation wavelength e) D, G, and 2D bands. f) Radial breathing mode region.

DOI: 10.1002/smll.201102173

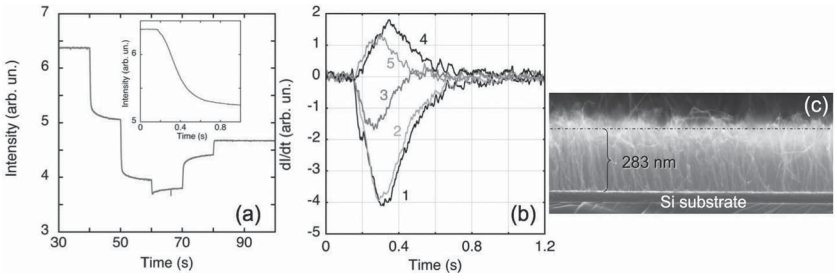

Figure 3. a) In-situ TRR data measured for a short SWNT array grown by five C_2H_2 pulses. Inset shows magnified view of the reflectivity signal during the first pulse. b) Derivatives of each TRR transient plotted starting from the valve opening times ($t = 0$) permit the comparison of the nucleation and growth kinetics on each pulse. c) Cross-sectional SEM image of the corresponding nanotube array.

In the case of relatively short gas pulses, and slow growth when at least a few pulses are required to reach an interference minimum, the changes in reflectivity, *dI*/*dt*, reflect the growth kinetics of carbon nanotubes. For example, in the case of coordinated growth, the derivative for the successive gas pulses changes sign from negative (curves 1, 2, 3) to positive (curves 4, 5) due to Fabry–Perot oscillations in the reflected intensity. As it will be shown, this is not the case for uncoordinated growth where the reflectivity does not oscillate, but only declines with time due to absorption and scattering. Another interesting observation is a double peak structure within the first reflectivity pulse, which corresponds to the initial exposure of virgin catalyst nanoparticles to a gas pulse.

To understand the time evolution of the reflectivity pulses for coordinated and uncoordinated growth, we compared them to the temporal profile of a C_2H_2 gas pulse obtained from our modeling of the pulsed CVD reactor. In the case of coordinated growth, the first gas pulse generates a double peak feature with the second peak delayed relative to the calculated gas pulse (**Figure 4**a). The two subsequent reflectivity pulses exhibit only the second, delayed peak with almost the same shape and intensity, and are broader than the calculated gas pulse. In the case of uncoordinated growth, the intensity of the second peak is relatively low and appears as a shoulder on the pronounced first peak of the first gas pulse (Figure 4b). Moreover, the total width is comparable to the calculated gas pulse width and is narrower than that for coordinated growth. In these cases, growth typically stops quickly as indicated by the lack of reflectivity changes after a few additional gas pulses (e.g., 10 more C_2H_2 pulses, see Supporting information (SI), Figure S1 and S2).

Detailed analysis of other coordinated and uncoordinated growth runs showed similar behavior, which can be summarized as follows: 1) In all cases, the derivative of the first gas pulse exhibits two peaks, i.e., a sharp peak at the leading edge of the gas pulse followed by a broader, delayed peak, which extends beyond the tail of the modeled gas pulse. 2) All subsequent pulses show only the second peak. 3) The relative intensities of these two peaks vary considerably, depending on the growth run.

The observed double-peak feature in the evolution of the growth rate, dI/dt, can be interpreted in the context of autocatalytic kinetics for both nanotube nucleation and growth processes, where in both cases induction delays are explained by the time required to form intermediate species which accelerate chemical conversion of the feedstock gas. Such autocatalytic kinetics result in "S-shaped" growth curves, with a slow induction period during the buildup of the necessary intermediates, a period of rapid and efficient reaction, and finally a period of decline as the chemical reactions terminate due to lack of reactants or available sites. Such "S-shaped" growth kinetics have been observed in carbon fiber[55] and nanotube[35] growth experiments for years, and more recently in the growth of carbon nanotube arrays.[56–58] However, separating the kinetics of nucleation and growth has been difficult until now.

Recently, Latorre et al.[54] developed a phenomenological autocatalytic model to describe "S-shaped" kinetics in the growth of nanotube forests measured by in-situ Raman spectroscopy. The model used the framework of growth by dissolution-precipitation driven by the gradient of carbon concentrations at the metal catalyst nanoparticle surface. First, however, the chemical reactions required for the nucleation and growth of a stable nanotube "cap" were considered, followed by the processes for cap liftoff and nanotube growth. The termination phase for nanotube nucleation resulted from the lack of available sites on a catalyst nanoparticle, while the termination of nanotube growth could be due to a variety of different reasons[19,21,44,52,59–61] including chemical reactions, such as those discussed by Eres et al.[57] to explain the preferential self-assembly of acetylene by autocatalytic reactions.[53]

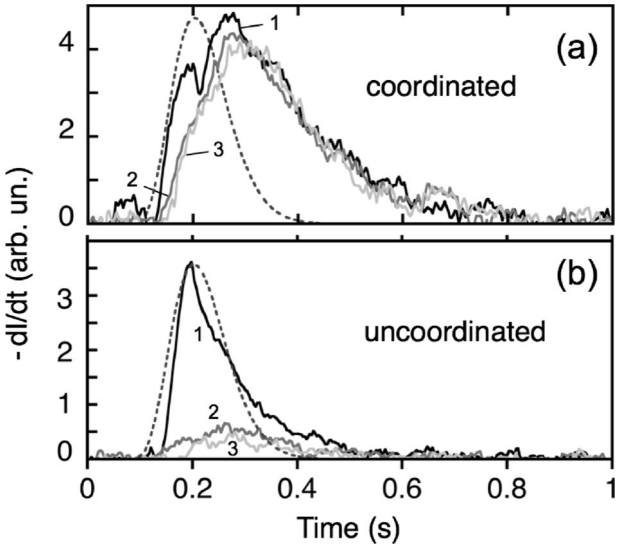

Figure 4. Derivatives of in-situ TRR signals, -dI/dt, for the first three C_2H_2 pulses (1–3) measured for a) coordinated growth, curve 1 in Figure 1a, and b) uncoordinated growth, in the Figure S1 of the SI. The dashed line is the calculated shape of the C_2H_2 gas pulse at the substrate (see Figure 9c), indicating that growth continues in a coordinated mode after the gas is gone.

DOI: 10.1002/smll.201102173

small NANO MICRO

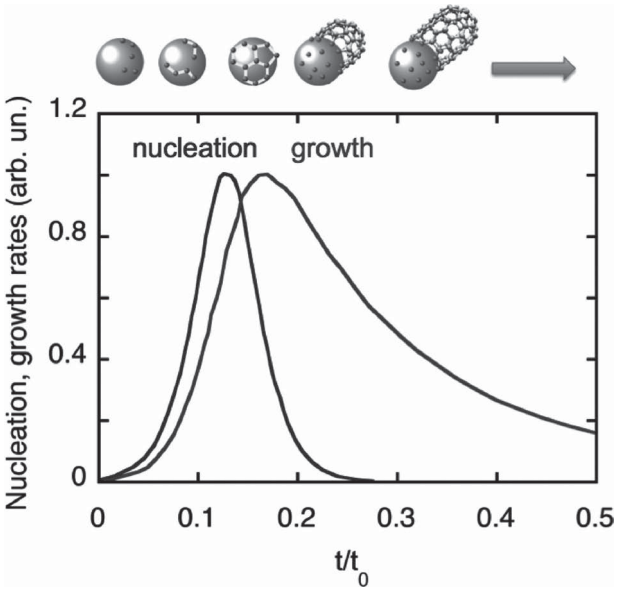

Figure 5. Kinetic rates predicted for carbon nanotube nucleation and growth based on autocatalytic reaction mechanisms.[54] The leading edge of the growth curve is determined by the integral of the nucleation curve, while the trailing edge depends on the lifetime of the growth process, t_0, which is either determined by natural termination mechanisms (e.g., due to catalyst deactivation ~10–100 min) or intentional cutoff of a feedstock gas (e.g., by pulsing t_0 = ~0.1–1 s, t_0 = 0.75 s as shown).

The time evolution of nanotube nucleation and growth should therefore show two rates with the fastest one due to the nucleation step—e.g., due to cap or intermediates formation—followed by the slower one due to nanotube growth (**Figure 5**). In typical in-situ experiments, usually only the second (growth) rate is resolved by measuring the intensities of the characteristic nanotube Raman bands,[56] for example, or by directly measuring nanotube lengths with TEM.[35] However, in-situ TRR allows one to monitor *both* events since deposition of even a single layer of graphene, for example, on a metal surface will give rise to a few percent change in reflectivity.[62] Indeed, we were able to observe *both* the nucleation and growth components (Figure 5) in situ during pulsed CVD of nanotube arrays, and to resolve them in the derivatives of the TRR signal, which reflects the evolution of the nucleation and growth rates of the array. The full width at half-maximum (FWHM) of the fastest component allows one to estimate the duration of the nucleation period, which was ~ 50 ms in the present case. The lack of the first component on subsequent gas pulses can be explained by the fact that the growth during these gas pulses does not require a nucleation step (cap formation), and can instead proceed by continued feeding of the existing Fe–C interface at a catalyst nanoparticle. This is consistent with our HR-TEM observations of continuous nanotubes without multiple caps forming during each gas pulse (Figure 2a,b).

Another interesting feature distinguishing coordinated and uncoordinated growth is the temporal widths of the corresponding reflectivity transients (Figure 4a,b). In the case of uncoordinated growth (Figure 4b), the width of the reflectivity transient matches that of the calculated gas pulse, but in the case of coordinated growth (Figure 4a) the reflectivity pulse is broader than the C_2H_2 pulse, which implies that some growth occurs after the gas pulse. This sustained growth may arise from the delayed arrival of hydrocarbon feedstock adsorbed on the surface of the alumina support due to diffusion and chemical reactions such as those suggested in reference [63].

To understand the origin of coordinated growth, we exposed identical catalyst films to different numbers of C_2H_2 gas pulses. Interestingly, even for seemingly identical conditions, we did not observe coordinated growth in all cases. **Figure 6** shows the cross-sectional SEM images and the corresponding reflectivity curves for nanotube arrays that exhibit coordinated behavior (18 pulse array), and show only random uncoordinated growth (15 pulse array) according to either the evolution or lack of Fabry–Perot oscillations in the TRR signal, respectively.

Although observation of interference fringes during in-situ monitoring is an excellent indication of coordinated growth, the process is highly protracted in pulsed CVD at the low feedstock fluxes because so many pulses are required to accumulate 300 nm of height required for the first TRR fringe to be observed. However, the derivatives of TRR signals can be used to predict coordinated versus uncoordinated growth. For example, on the basis of the TRR signals in the 5-pulse experiment of Figure 6, we can determine that growth will proceed in a coordinated mode as follows.

Figure 7a,b summarize the derivatives of the TRR signals, ($-dI/dt$), for the first and the second C_2H_2 pulses for all of the growth experiments discussed above. All of the curves in Figure 7a,b are normalized to the intensity of the first (fast) peak in Figure 7a. Close inspection reveals that the set of curves for the first and the second C_2H_2 gas pulses are quite different for coordinated and uncoordinated growth. For example, all of the arrays that grew in a coordinated fashion have a pronounced second peak on the first C_2H_2 pulse, the intensity of which is larger when the growth proceeds faster.

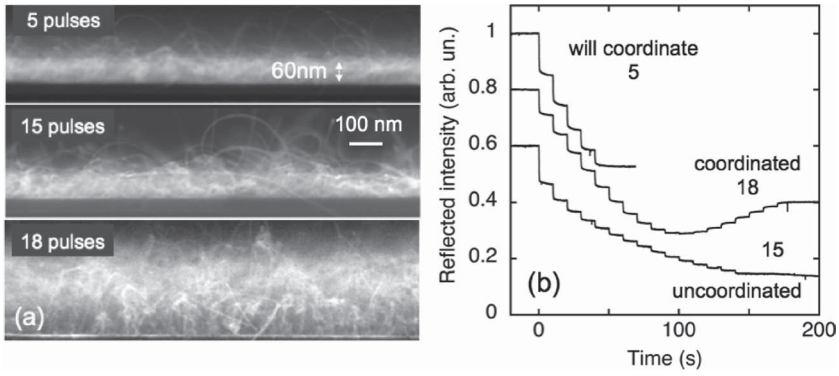

Figure 6. a) Cross-sectional SEM images, and b) corresponding reflectivity signals for three cases of nanotube nucleation and growth using different number of gas pulses ranging from 5 to 18. Note that the two lower TRR signals are offset by 0.2 and 0.4, respectively, from their maximum value of 1.0 for clarity.

DOI: 10.1002/smll.201102173

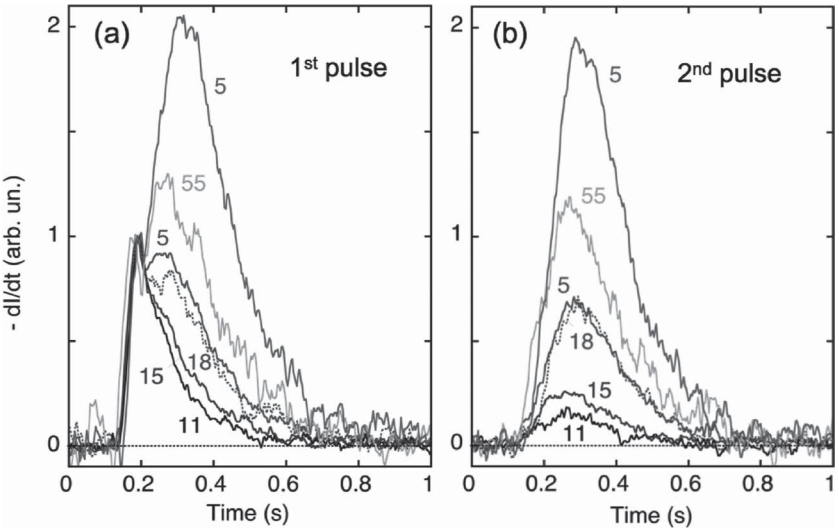

Figure 7. A summary of derivatives, $-dI/dt$, of in-situ TRR curves measured in six different experiments for catalysts exposed to a) the first, and b) the second C_2H_2 gas pulses. Each curve is labeled with the number of gas pulses used for the corresponding growth runs: 11 and 15 pulses are uncoordinated growth (Figure 4b and 6b); 18 (dotted lines) is borderline coordinated growth (Figure 6b, rate 15 nm/pulse); and 5, 55, and 5 are coordinated (aligned) growth (Figure 6b; Figure 4a, rate 30 nm/pulse; and Figure 3a,b, rate 60 nm/pulse, respectively), where a pronounced delayed second peak is evident in (a). All curves in (a) and (b) are normalized to the intensity of the corresponding fast peaks in (a).

This is not the case for uncoordinated growth, in which the second component is missing during the first gas pulse (curves 11 and 15 in Figure 7a). The uncoordinated cases also have very small changes in reflectivity on the second (curves 11 and 15 in Figure 7b) and subsequent gas pulses compared to those on the first gas pulse, which further indicates that the growth does not develop well in these cases. Furthermore, in all cases of successful coordinated growth (curves 5, 55, 5, and 18 in Figure 7a) the 2nd reflectivity pulse for the same runs have intensities comparable to the second component observed on the 1st gas pulse, which indicates that incremental, coordinated growth continue to develop in these cases.

Therefore the reflectivity signal for the *first gas pulse* can be used to predict if coordinated growth will develop during subsequent pulsing. The key predictor is the double-peak feature of the first dI/dt pulse (Figure 4a and Figure 7a). Indeed, the development of the second peak with an intensity comparable to or exceeding that of the first peak on the first gas pulse indicates that a sufficient fraction of the ensemble of catalyst nanoparticles has nucleated and begun the growth of nanotubes with an areal density required to support coordinated growth of an array. The relative intensities of the first and the second peaks in the derivatives of the TRR signals (Figure 7a) could serve as a qualitative indication of the future development of the growth in the coordinated mode. When the intensity of the second peak is small compared to the borderline case, e.g., in the case of the 18-pulse curve, the growth does not develop as coordinated.

In summary, these measurements performed on the borderline of effective coordinated growth can be understood in the context of an autocatalytic model[54] for nucleation and growth assuming that catalyst nanoparticles have different catalytic activities and therefore respond differently to the feedstock flux. In the autocatalytic model, the nucleation and growth rates are proportional to feedstock flux. As illustrated in **Figure 8** increasing the feedstock flux can drive the reaction to completion within time t_0, which is revealed in pulsed growth. For low feedstock fluxes only a relatively small fraction of catalyst nanoparticles within an ensemble can effectively nucleate and grow nanotubes during the gas pulse (nucleation curve). As a result, the nucleation density is too low to support coordinated growth by crowding. However, increasing the feedstock flux (or catalytic activity of the particles) decreases the induction times for nucleation and growth such that both can occur within the gas pulse.[32] If the flux is too high, growth can be driven to termination, as observed in reference [[32]] for the most catalytically active, small-diameter nanoparticles, leading to banded arrays with variable density (termination curve). However, if the flux and width of the gas pulse are chosen appropriately to match the activity of the catalyst, nucleation and growth of a large fraction of nanoparticles can occur within the gas pulse while avoiding termination (growth curve), thereby enabling the incremental growth of continuous nanotubes on subsequent pulses.

3. Conclusion

Fast, well-defined (0.2 s) pulses of acetylene and time-resolved reflectivity were used to incrementally grow short SWNT arrays and simultaneously measure their nucleation and growth kinetics on very short timescales. The derivative of the TRR signal exhibits an interesting double-peak temporal feature during exposure of the catalyst to the first

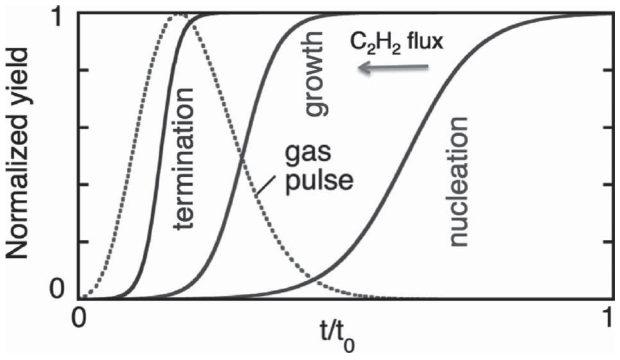

Figure 8. Calculated S-shaped kinetic curves for nanotube growth based on an autocatalytic model.[53,54] Increasing the C_2H_2 flux drives the kinetics to completion in different times (t_0, $0.5t_0$, $0.25t_0$ pictured) allowing either nucleation, growth, or termination of growth within the duration of the gas pulse in pulsed CVD.

small 2012,
DOI: 10.1002/smll.201102173

small NANO MICRO

C_2H_2 pulse—a fast (~50 ms) peak—which was attributed to formation of the initial nanotube cap, and a slower component that extends beyond the temporal width of the gas pulse and is attributed to array growth involving intermediate species. The relative intensity of these nucleation and growth peaks were shown to correspond to the total nanotube nucleation density and growth rate, as well as serve as a predictor of the future development of the growth on successive C_2H_2 pulses into a coordinated array.

Incremental growth of carbon nanotube arrays by pulsed CVD is interpreted in the context of an autocatalytic kinetic model as a special processing window in which sufficiently high fluxes of feedstock gas drive the nucleation and rapid growth phases of a catalyst nanoparticle ensemble to occur within the temporal period of the gas pulse without inducing growth termination. Using this approach, we demonstrated that SWNTs without noticeable kinks, caps, or sidewall defects could be grown incrementally into coordinated arrays in steps as small as 25 nm, to heights as small as 60 nm and as tall as 1.5 μm. An estimated 98% of the nanotubes regrow on each successive pulse, permitting incremental growth of arrays involving up to 100 pulses. Predictive incremental growth using pulsed CVD controlled by in-situ TRR opens new possibilities for the precise, synthesis of short SWNT arrays for a variety of biological, thermal, optoelectronic, and sensing applications.

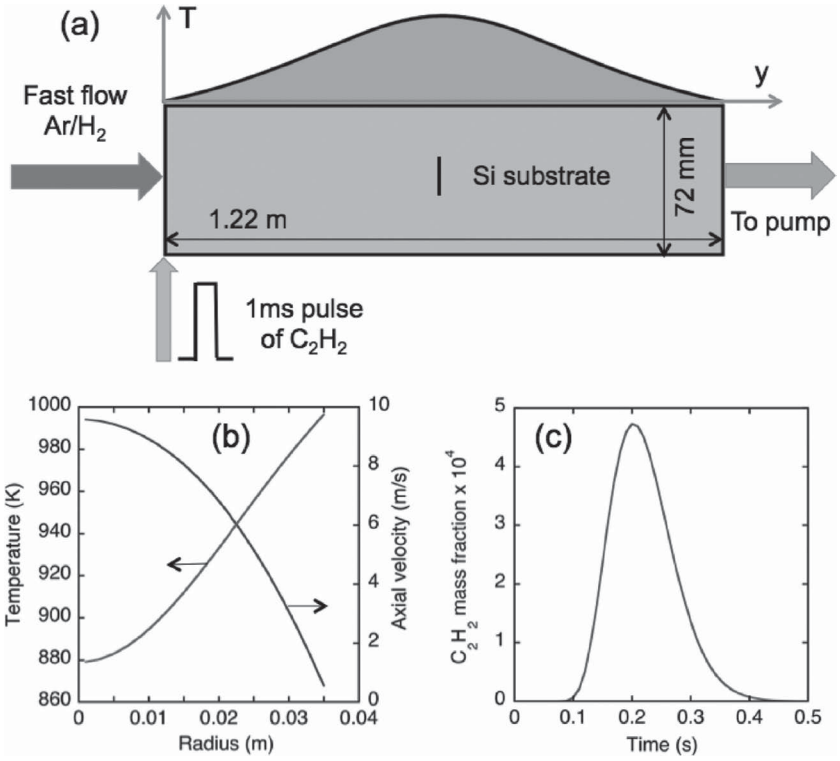

Figure 9. a) Schematic of the pulsed CVD reactor geometry used in the experiment and modeling. Fast continuous flow of Ar/H_2 is introduced into a quartz tube through mass-flow controllers at 2000/250 sccm, respectively. The other end of the tube is pumped down and a stationary pressure of 6.3 Torr is maintained at this end. C_2H_2 is injected into the Ar/H_2 flow through a pulsed valve (1 ms pulse width). A Si-substrate with a catalyst film is located in the center of the quartz tube. The curve at the top shows the temperature profile along the walls of the quartz tube, which is varied from 300 K at the ends to 1000 K at the center of the tube. b) Radial profiles of the gas temperature and the axial velocity at the center of the quartz tube at $t = 0.2$ s after the valve was actuated. c) Calculated shape of C_2H_2 gas pulse at the substrate location.

4. Experimental Section

CVD Reactor: The experimental apparatus used for the pulsed CVD growth of carbon nanotube arrays has been described elsewhere.[44] **Figure 9**a shows the schematic of our CVD reactor. For pulsed growth, Ar (2000 sccm) and H_2 (250 sccm) were flowed continuously at a total pressure of 6.3 Torr at ~700 °C. Acetylene gas was injected from a pulsed valve (Parker, model 099-0340-900 with orifice diameters of 0.76 mm), which was actuated by a circuit triggered by a digital delay generator (Stanford Research Systems, SR545) and could be opened for a minimum time of 1 ms. The repetition rate of the gas pulses was 0.1 Hz and the onset of valve opening was recorded simultaneously with the TRR signal using a small piezoelectric microphone attached to the valve. The peak partial pressures of C_2H_2 as a function of different backing pressures supplied to the valve were estimated using measurements of the C_2H_2 pressure rise per pulse in the evacuated CVD reactor at room temperature. The pressure per pulse was then converted to standard cubic centimeters per pulse using the calibrated volume of the CVD reactor, which gave 0.2 cm^3 of acetylene at 20 psi backing pressure. Assuming the duration of the gas pulse at the substrate was ~0.2 s FWHM (estimated from transients in the optical reflectivity signals), we determined a peak flow of 60 sccm, or a partial pressure of 0.16 Torr in the peak of the gas pulse. The peak acetylene partial pressure in a pulse was varied by adjusting the backing gas pressure of acetylene to the valve, the gate width of the applied electrical pulse, and by choosing a particular valve orifice.

Calculated Gas Dynamics: To understand the dynamics of the feedstock gas propagation, i.e., the arrival time to the substrate, as well as the shape and the width of the C_2H_2 pulses at the substrate location, modeling of the CVD reactor was performed (see SI, section 3). Figure 9b show the radial profiles of the temperature and velocity at the center of the quartz tube 0.2s after the valve was opened. Note that this corresponds to the maximum of the C_2H_2 pulse at the substrate location. One can see that the axial velocity at the center is very high, ~10 m/s. The temperature at the center of the quartz tube is about 880K which is slightly lower than the maximum wall temperature ~1000 K.

At these conditions, the most probable velocity and the mean free path of acetylene molecules at the center of the quartz tube are ~7.5×10^4 cm/s and ~24 μm, respectively. According to this calculation the C_2H_2 gas pulse (Figure 9c) is relatively narrow (~120 ms FWHM) with a sharp leading edge, which arrives at the substrate

DOI: 10.1002/smll.201102173

100 ms after actuation of the valve. A more detailed description of this model is given in the SI. These calculations show that the shape and duration of the gas pulse will allow one to study fast nucleation and growth kinetics occurring within times <100 ms.

Catalyst Preparation: To grow carbon nanotube arrays using the setup described above, we used Si(100) wafer substrates with an e-beam evaporated 30-nm buffer layer of Al_2O_3 and Fe catalyst of nominal thickness 0.5 nm.

Optical Reflectivity Measurements: A HeNe laser at 633 nm was used to illuminate a vertically standing substrate in the tube furnace. The specularly reflected beam was turned by a mirror, passed through a lens and bandpass filter, and detected with a fast photodiode. The photodiode intensity was digitized (12-bit) at 300 points/s.[44] Every reflectivity curve showing interference fringes was calibrated using the arrested growth approach[26,44] and cross sectional SEM imaging to determine the array length per an interference fringe. This resulted in 286 ± 20 nm/fringe for curve 1 in Figure 1a with the SEM shown in Figure 2c; 283 ± 20 nm/fringe for the reflectivity curve in Figure 3a with the corresponding SEM in Figure 3c; and 281 ± 30 nm for the 18-pulses curve in Figure 6b with the SEM in Figure 6a (18 pulses case). Within the error bars these values are close to those derived for the SWNT arrays grown by pulsed CVD in our previous work using two different calibration approaches, i.e., marking of SWNT arrays with horizontal stripes, which resulted in 300 ± 20 nm/fringe and directly deriving the effective refractive index ($n_{eff} = 1.073$), and using complete fitting of the reflectivity curves, which resulted in 295 ± 20 nm/fringe.

Ex-Situ Characterization: The nanotube arrays on Si substrates were typically cleaved at a position that included the optically monitored spot, and investigated by scanning electron microscopy (Hitachi S-4700 FEG-SEM at ~2 kV). Strips of the array from the cleaved region were transferred to TEM grids for analysis by either Z-contrast STEM (Hitachi HD-2000 at 200 kV) or bright- field TEM imaging (Hitachi HF-2000 at 200 kV). Confocal micro-Raman spectroscopy capable of measuring large-diameter SWNTs grown in arrays was performed on the sides of the cleaved arrays using a Jobin-Yvon T64000 triple monochromator system and 532 nm laser excitation.

Supporting Information

Supporting Information is available from the Wiley Online Library or from the author.

Acknowledgements

Synthesis science sponsored by the Division of Materials Sciences and Engineering, Office of Basic Energy Sciences, U.S. Department of Energy. Characterization science including Raman spectroscopy, SEM, and HR TEM part of this research was conducted at the Center for Nanophase Materials Sciences and at the Shared Research Equipment (ShaRE) user facility, which are sponsored at Oak Ridge National Laboratory by the Division of Scientific User Facilities, U.S. Department of Energy.

[1] I. Ivanov, A. Puretzky, G. Eres, H. Wang, Z. W. Pan, H. T. Cui, R. Y. Jin, J. Howe, D. B. Geohegan, *Appl. Phys. Lett.* **2006**, *89*, 223110.
[2] X. J. Hu, A. A. Padilla, J. Xu, T. S. Fisher, K. E. Goodson, *J. Heat. Trans.* **2006**, *128*, 1109.
[3] M. Akoshima, K. Hata, D. N. Futaba, K. Mizuno, T. Baba, M. Yumura, *Jpn. J. Appl. Phys.* **2009**, *48*, 05EC07.
[4] Z. L. Gao, K. Zhang, M. M. F. Yuen, *Nanotechnology* **2011**, *22*, 445611.
[5] A. Izadi-Najafabadi, T. Yamada, D. N. Futaba, M. Yudasaka, H. Takagi, H. Hatori, S. Iijima, K. Hata, *ACS Nano* **2011**, *5*, 811.
[6] A. Izadi-Najafabadi, S. Yasuda, K. Kobashi, T. Yamada, D. N. Futaba, H. Hatori, M. Yumura, S. Iijima, K. Hata, *Adv. Mater.* **2010**, *22*, E235.
[7] Y. Awano, S. Sato, M. Nihei, T. Sakai, Y. Ohno, T. Mizutani, *Proc. IEEE* **2010**, *98*, 2015.
[8] C. L. Pint, Y. Q. Xu, M. Pasquali, R. H. Hauge, *ACS Nano* **2008**, *2*, 1871.
[9] T. Y. Tsai, C. Y. Lee, N. H. Tai, W. H. Tuan, *Appl. Phys. Lett.* **2009**, *95*, 013107.
[10] A. Modi, N. Koratkar, E. Lass, B. Q. Wei, P. M. Ajayan, *Nature* **2003**, *424*, 171.
[11] K. Mizuno, J. Ishii, H. Kishida, Y. Hayamizu, S. Yasuda, D. N. Futaba, M. Yumura, K. Hata, *Proc. Natl. Acad. Sci. USA* **2009**, *106*, 6044.
[12] Z. P. Yang, L. J. Ci, J. A. Bur, S. Y. Lin, P. M. Ajayan, *Nano Lett.* **2008**, *8*, 446.
[13] L. Ge, S. Sethi, L. Ci, P. M. Ajayan, A. Dhinojwala, *Proc. Natl. Acad. Sci. USA* **2007**, *104*, 10792.
[14] L. Qu, L. Dai, *Adv. Mater.* **2007**, *19*, 3844.
[15] L. T. Qu, L. M. Dai, M. Stone, Z. H. Xia, Z. L. Wang, *Science* **2008**, *322*, 238.
[16] A. Y. Cao, P. L. Dickrell, W. G. Sawyer, M. N. Ghasemi-Nejhad, P. M. Ajayan, *Science* **2005**, *310*, 1307.
[17] M. Zhang, K. R. Atkinson, R. H. Baughman, *Science* **2004**, *306*, 1358.
[18] H. S. Peng, M. Jain, Q. W. Li, D. E. Peterson, Y. T. Zhu, Q. X. Jia, *J. Am. Chem. Soc.* **2008**, *130*, 1130.
[19] A. A. Puretzky, G. Eres, C. M. Rouleau, I. N. Ivanov, D. B. Geohegan, *Nanotechnology* **2008**, *19*, 055605.
[20] C. M. Rouleau, G. Eres, H. Cui, H. M. Christen, A. A. Puretzky, D. B. Geohegan, *Appl. Phys. A* **2008**, *93*, 1005.
[21] E. R. Meshot, A. J. Hart, *Appl. Phys. Lett.* **2008**, *92*, 113107.
[22] K. Hata, D. N. Futaba, K. Mizuno, T. Namai, M. Yumura, S. Iijima, *Science* **2004**, *306*, 1362.
[23] P. B. Amama, C. L. Pint, L. McJilton, S. M. Kim, E. A. Stach, P. T. Murray, R. H. Hauge, B. Maruyama, *Nano Lett.* **2009**, *9*, 44.
[24] C. L. Pint, S. T. Pheasant, A. N. G. Parra-Vasquez, C. Horton, Y. Q. Xu, R. H. Hauge, *J. Phys. Chem. C* **2009**, *113*, 4125.
[25] C. T. Wirth, C. Zhang, G. F. Zhong, S. Hofmann, J. Robertson, *ACS Nano* **2009**, *3*, 3560.
[26] D. B. Geohegan, A. A. Puretzky, I. N. Ivanov, S. Jesse, G. Eres, J. Y. Howe, *Appl. Phys. Lett.* **2003**, *83*, 1851.
[27] T. Iwasaki, J. Robertson, H. Kawarada, *Nano Lett.* **2008**, *8*, 886.
[28] K. Liu, K. L. Jiang, C. Feng, Z. Chen, S. Fan, *Carbon* **2005**, *43*, 2850.
[29] X. S. Li, A. Y. Cao, Y. J. Jung, R. Vajtai, P. M. Ajayan, *Nano Lett.* **2005**, *5*, 1997.
[30] S. Maruyama, E. Einarsson, Y. Murakami, T. Edamura, *Chem. Phys. Lett.* **2005**, *403*, 320.
[31] J. J. Jackson, A. A. Puretzky, K. L. More, C. M. Rouleau, G. Eres, D. B. Geohegan, *ACS Nano* **2010**, *4*, 7573.
[32] D. B. Geohegan, A. A. Puretzky, J. J. Jackson, C. M. Rouleau, G. Eres, K. L. More, *ACS Nano* **2011**, *5*, 8311.
[33] S. Helveg, C. Lopez-Cartes, J. Sehested, P. L. Hansen, B. S. Clausen, J. R. Rostrup-Nielsen, F. Abild-Pedersen, J. K. Norskov, *Nature* **2004**, *427*, 426.
[34] J. A. Rodriguez-Manzo, M. Terrones, H. Terrones, H. W. Kroto, L. T. Sun, F. Banhart, *Nat. Nanotechnol.* **2007**, *2*, 307.

DOI: 10.1002/smll.201102173

[35] M. Lin, J. P. Y. Tan, C. Boothroyd, K. P. Loh, E. S. Tok, Y. L. Foo, *Nano Lett.* **2006**, *6*, 449.
[36] R. Sharma, Z. Iqbal, *Appl. Phys. Lett.* **2004**, *84*, 990.
[37] R. Sharma, E. Moore, P. Rez, M. M. J. Treacy, *Nano Lett.* **2009**, *9*, 689.
[38] R. Sharma, P. Rez, M. Brown, G. H. Du, M. M. J. Treacy, *Nanotechnology* **2007**, *18*, 125602.
[39] R. Sharma, P. Rez, M. M. J. Treacy, S. J. Stuart, *J. Electron. Microsc.* **2005**, *54*, 231.
[40] A. Gamalski, E. S. Moore, M. M. J. Treacy, R. Sharma, P. Rez, *Appl. Phys. Lett.* **2009**, *95*, 233109.
[41] H. Yoshida, T. Shimizu, T. Uchiyama, H. Kohno, Y. Homma, S. Takeda, *Nano Lett.* **2009**, *9*, 3810.
[42] H. Yoshida, S. Takeda, T. Uchiyama, H. Kohno, Y. Homma, *Nano Lett.* **2008**, *8*, 2082.
[43] D. H. Kim, H. S. Jang, C. D. Kim, D. S. Cho, H. S. Yang, H. D. Kang, B. K. Min, H. R. Lee, *Nano Lett.* **2003**, *3*, 863.
[44] A. A. Puretzky, D. B. Geohegan, S. Jesse, I. N. Ivanov, G. Eres, *Appl. Phys. A-Mater.* **2005**, *81*, 223.
[45] E. Einarsson, Y. Murakami, M. Kadowaki, S. Maruyama, *Carbon* **2008**, *46*, 923.
[46] Y. Murakami, Y. Miyauchi, S. Chiashi, S. Maruyama, *Chem. Phys. Lett.* **2003**, *377*, 49.
[47] S. Chiashi, Y. Murakami, Y. Miyauchi, S. Maruyama, *Chem. Phys. Lett.* **2004**, *386*, 89.
[48] K. Kaminska, J. Lefebvre, D. G. Austing, P. Finnie, *Nanotechnology* **2007**, *18*, 165707.
[49] M. Picher, E. Anglaret, R. Arenal, V. Jourdain, *Nano Lett.* **2009**, *9*, 542.
[50] P. Finnie, A. Li-Pook-Than, J. Lefebvre, *Nano Res.* **2009**, *2*, 783.
[51] P. Vinten, J. Lefebvre, P. Finnie, *Chem. Phys. Lett.* **2009**, *469*, 293.
[52] P. Vinten, P. Marshall, J. Lefebvre, P. Finnie, *Nanotechnology* **2010**, *21*, 035603.
[53] M. Frenklach, D. Clary, *Ind. Eng. Chem. Fund.* **1983**, *22*, 433.
[54] N. Latorre, E. Romeo, F. Cazana, T. Ubieto, C. Royo, J. J. Villacampa, A. Monzon, *J. Phys. Chem. C* **2010**, *114*, 4773.
[55] R. T. K. Baker, M. A. Barber, R. J. Waite, P. S. Harris, F. S. Feates, *J. Catal.* **1972**, *26*, 51.
[56] A. Li-Pook-Than, J. Lefebvre, P. Finnie, *J. Phys. Chem. C* **2010**, *114*, 11018.
[57] G. Eres, C. M. Rouleau, M. Yoon, A. A. Puretzky, J. J. Jackson, D. B. Geohegan, *J. Phys. Chem. C* **2009**, *113*, 15484.
[58] G. Eres, A. A. Kinkhabwala, H. T. Cui, D. B. Geohegan, A. A. Puretzky, *J. Phys. Chem. B* **2005**, *109*, 16684.
[59] M. Stadermann, S. P. Sherlock, J. B. In, F. Fornasiero, H. G. Park, A. B. Artyukhin, Y. M. Wang, J. J. De Yoreo, C. P. Grigoropoulos, O. Bakajin, A. A. Chernov, A. Noy, *Nano Lett.* **2009**, *9*, 738.
[60] S. M. Kim, C. L. Pint, P. B. Amama, R. H. Hauge, B. Maruyama, E. A. Stach, *J. Mater. Res.* **2010**, *25*, 1875.
[61] M. Bedewy, E. R. Meshot, H. C. Guo, E. A. Verploegen, W. Lu, A. J. Hart, *J. Phys. Chem. C* **2009**, *113*, 20576.
[62] K. S. Novoselov, *Rev. Mod. Phys.* **2011**, *83*, 837.
[63] A. Magrez, R. Smajda, J. W. Seo, E. Horvath, P. R. Ribic, J. C. Andresen, D. Acquaviva, A. Olariu, G. Laurenczy, L. Forro, *ACS Nano* **2011**, *5*, 3428.

Received: October 14, 2011
Revised: December 13, 2011
Published online: